ACS APPLIED MATERIALS & INTERFACES

www.acsami.org

Research Article

Skeleton Engineering of Homocoupled Conjugated Microporous Polymers for Highly Efficient Uranium Capture via Synergistic Coordination

Lei Zhang, Ning Pu, Boxuan Yu, Gang Ye,* Jing Chen, Shengming Xu,* and Shengqian Ma*

Cite This: *ACS Appl. Mater. Interfaces* 2020, 12, 3688−3696

Read Online

ACCESS | Metrics & More | Article Recommendations | Supporting Information

ABSTRACT: Developing efficient adsorbents for uranium enrichment is of great significance for resource sustainability and environmental safety. This study presents a facile and adaptable post-synthetic strategy to prepare highly efficient uranium adsorbents via engineering the π-conjugated skeletons of homocoupled conjugated microporous polymers (HCMPs). Taking advantage of the diyne units in the π-conjugated skeletons, bis-amidoxime uranophiles, one of the state-of-the-art ligands of uranyl ions, were introduced to the frameworks of HCMPs. The functionalized HCMPs preserved the interconnected 3D microporous networks and rigid conjugated skeletons with abundant bis-amidoxime ligands uniformly distributed in the pore channels. Such structural advantages of the adsorbents afforded very fast adsorption kinetics within 15 min to reach the equilibrium and high capacity of uranium (450 mg/g). Moreover, DFT calculation suggests a synergistic coordination as the most energetically favored coordination mode of the uranyl/bis-amidoxime complexes. This study contributes new insights into the underlying mechanism responsible for the highly efficient adsorption ability of the bis-amidoxime-functionalized HCMPs toward uranium. Meanwhile, the synthetic methodology established here could be extended to task-specific design and skeleton engineering of more functional HCMPs for broadened applications.

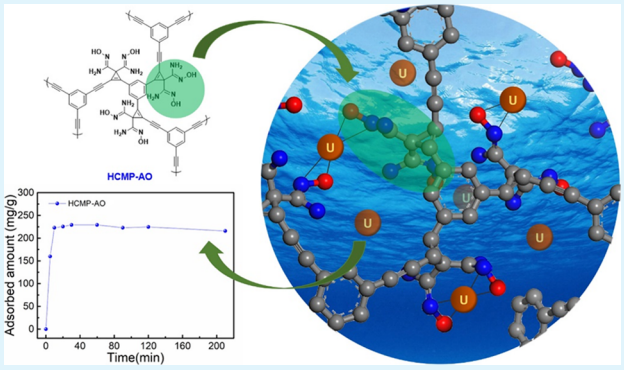

KEYWORDS: *homocoupled conjugated microporous polymer (HCMP), adsorption, amidoxime, uranium, density functional theory (DFT)*

1. INTRODUCTION

Uranium as a strategic resource plays a pivotal role in nuclear energy development. Due to the uranium deficiency in geological reserves, substantial efforts are being made worldwide to develop technologies for uranium extraction from seawater to secure the nuclear energy production because oceans contain nearly 1000 times more uranium (~4.5 billion tons).[1−3] On the other hand, uranium-containing wastes or contaminants are widely generated in the nuclear fuel cycle as well as in nuclear accidents. Serious environmental concerns are raised due to the radioactivity and chemical toxicity of uranium.[4] Therefore, there is great motivation to develop cost- and energy-efficient methods for uranium enrichment and separation.[5]

Adsorption has been recognized as an effective and feasible way to reach this end.[6−15] However, the critical challenge lies in the extremely low concentration of uranium in above-mentioned environmental media, that is, 3 ppb in natural seawater, coexisting with a considerable amount of interfering metal ions.[16] Desirable properties of an ideal adsorbent material include high adsorption capacity, fast adsorption kinetics, good chemical stability, and excellent selectivity. Such criteria exclude some traditional porous adsorbent materials such as clays, activated carbons, and zeolites for industrial applications due to the slow adsorption kinetics and low adsorption capacity.[17,18] Although metal−organic framework based uranium adsorbents have been recently demonstrated to provide fast adsorption kinetics and high adsorption capacity,[19] further application of these materials remains a great challenge due to their poor stability in aqueous solutions.

Porous organic polymers (POPs), with features of large specific surface area, tunable pore size, and strong covalent linkages, represent a new generation of porous materials showing great potential for challenging energy and environmental issues.[20] In recent years, fascinating members in the POP family, including covalent organic frameworks

Received: November 18, 2019
Accepted: December 26, 2019
Published: December 26, 2019

https://dx.doi.org/10.1021/acsami.9b20944
ACS Appl. Mater. Interfaces 2020, 12, 3688−3696

Scheme 1. Synthetic Route of HCMP Functionalized with Bis-amidoxime Uranophiles

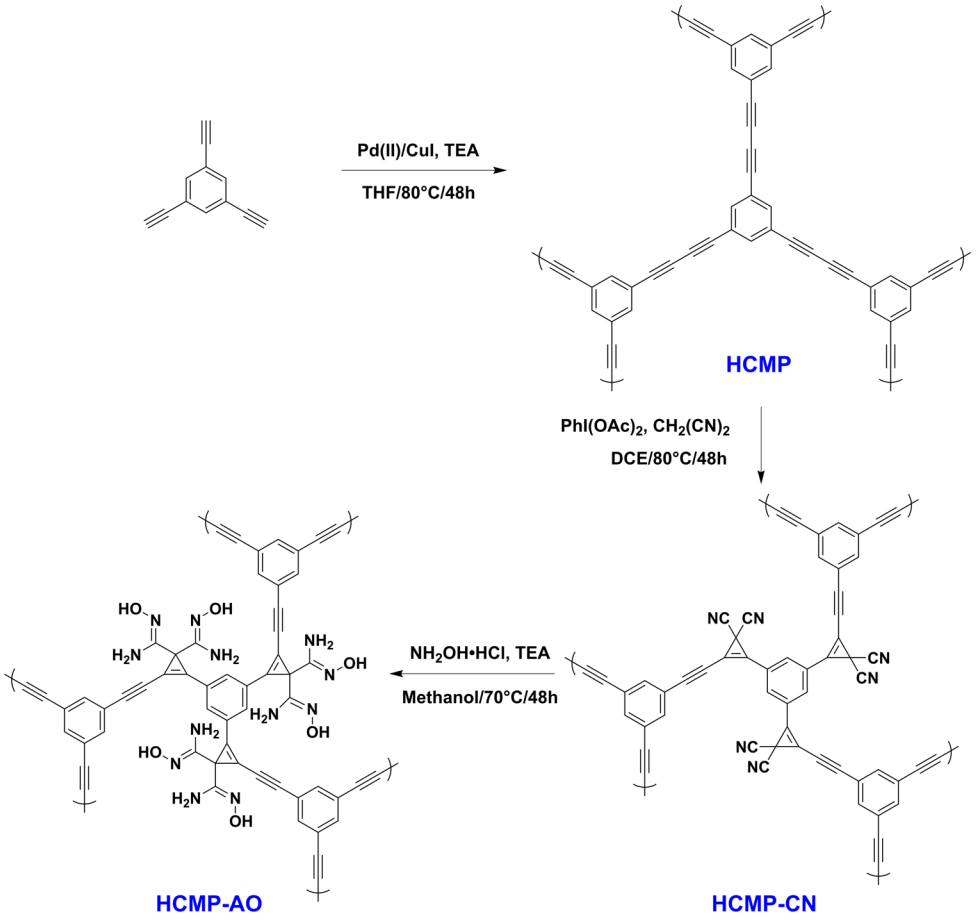

(COFs),[21−24] polymers of intrinsic microporosity,[25] conjugated microporous polymers (CMPs),[26] and porous aromatic frameworks (PAFs),[27,28] have been synthesized and exploited for applications in gas storage,[29−31] separation,[32,33] and catalysis.[34,35] The development of rationally designed POPs[36] including functionalized COFs[37] and PAFs[38,39] for efficient uranium adsorption has also been demonstrated.

As a unique category of porous materials, CMPs are featured by the abundant open and interconnected micropores in three-dimensional (3D) networks and all-rigid π-conjugated skeletons.[26] Since the first report by Cooper et al., these amorphous porous materials have received considerable research interest.[40,41] Their favorable physicochemical properties, tunable porosity, and especially the broad scope for facile anchoring of specific chelating ligands to the 3D networks make them ideal adsorbents for environmental applications. Hua's group has recently reported the architecture of two classes of CMPs based on 1,3,5-substituted benzene node connected by fluorene strut-bearing phosphate and amidoxime ligands for uranium adsorption and detection, achieving an optimal capacity of 73 mg/g in HNO_3 solutions[42] and a detection limit of 1.7×10^{-9} mol/L for uranyl ions in deionized water.[43] However, due to the different geometries of the building blocks and the steric hindrance of the ligand-bearing fluorene units, the CMPs obtained by cross-coupling reactions exhibited a low BET surface area (<100 m^2/g). Meanwhile, the accessibility of the ligands might be partially sacrificed because of the low porosity, which impeded the mass diffusion in the adsorption process.

Another synthetic strategy to construct CMPs is homocoupling of the same building blocks to form 3D microporous networks with conjugated skeletons.[44−46] These homocoupled CMPs (HCMPs) usually show improved BET surface area, well-defined porous frameworks and channels, and relatively narrow micropore size distribution. Meanwhile, the conjugated skeletons can serve as a favorable platform for post-functionalization via well-established synthetic chemistry, that is, thiol-yne click reaction,[47] to introduce desired functionalities, which broadens the opportunities for task-specific design and pore engineering of CMPs.

Herein, we present a facile and adaptable post-functionalization strategy to engineer the π-conjugated skeletons of HCMPs for preparing novel uranium adsorbents. Intrinsic HCMP with well-developed microporous 3D networks was synthesized via the homocoupling of 1,3,5-triethynylbenzene building blocks. Taking advantage of the diyne units in the π-conjugated skeletons, bis-amidoxime uranophiles, one of the state-of-the-art ligands of uranyl ions,[48−50] were introduced by an addition reaction with malononitrile followed by hydroxylamine treatment (Scheme 1). The functionalized HCMP (HCMP-AO) still maintained the interconnected microporous networks and rigid conjugated skeletons with abundant bis-amidoxime ligands uniformly distributed in the pore channels. Because of the structural advantages and high degree of functionality, HCMP-AO showed fast adsorption kinetics and high capacity toward uranyl ions. Besides, DFT calculation was employed to examine the interaction between HCMP-AO and uranyl ions, suggesting a synergistic coordination mode.

https://dx.doi.org/10.1021/acsami.9b20944
ACS Appl. Mater. Interfaces 2020, 12, 3688−3696

2. EXPERIMENTAL SECTION

2.1. Materials. Dichlorobis(triphenylphosphine)palladium(II) (98%), copper(II) phosphate (98%), tetrahydrofuran (THF, 99.8%, ACS/HPLC certified), triethylamine (TEA, 99%), iodobenzene diacetate (98%), malononitrile (99%), 1,2-dichloroethane (99%), arsenazo III (95%[t], spectrophotometric reagent for U, Th, Zr, and other metals, indicator for the precipitation titration of SO_4 with Ba), and L-(+)-tartaric acid (99%) were purchased from J&K Scientific and used as received. 1,3,5-Triethynylbenzene (98%) was purchased from Extension Scientific and used as received. Hydroxylamine hydrochloride (99%) was purchased from Sigma-Aldrich. Trichloromethane (98%), acetone (95%), nitric acid (69%), and sodium hydroxide (99%) were purchased from Beijing Chemical Works. Deionized water used in adsorption tests was purchased from Watsons and used as received. Uranyl nitrate hexahydrate $UO_2(NO_3)_2{\cdot}6H_2O$ was provided by the China Institute of Atomic Energy.

2.2. Synthesis of HCMP. 1,3,5-Triethynylbenzene (600 mg, 4.0 mmol), bis(triphenylphosphine)palladium(II) dichloride (85 mg, 3 mol %), and copper iodide (22 mg, 3 mol %) were dissolved in a mixture of THF (4.0 mL) and Et_3N (4.0 mL). The reaction mixture was heated to 70 °C and stirred for 36 h under a nitrogen atmosphere. The mixture was cooled to room temperature, and the precipitate was separated by filtration. Afterward, the precipitate was washed four times with chloroform, water, methanol, and acetone to remove the unreacted monomer and residual catalyst. Then the polymer was washed by Soxhlet extraction (methanol) for 2 days and dried in vacuum for 12 h at 50 °C.[44]

2.3. Synthesis of HCMP-CN. $PhI(OAc)_2$ (1.24 g, 3.8 mmol), malononitrile (0.606 g, 9.2 mmol), and HCMP (0.341 g) in dichloroethane (60 mL) were stirred at 80 °C for 48 h. After heating, the mixture was cooled to room temperature, and the precipitate was separated by filtration and then washed with dichloroethane and deionized water until the filtrate was colorless and nearly neutral. The precipitate was dried in vacuum for 12 h at 50 °C. The resulting product was denoted as HCMP-CN.

2.4. Synthesis of HCMP-AO. As a typical synthesis recipe, 0.2 g of HCMP-CN was swollen in 20 mL of methanol for 10 min followed by the addition of 0.5 g of $NH_2OH{\cdot}HCl$ and 0.75 g of Et_3N. After being stirred at 70 °C for 48 h, cyano groups were converted into amidoxime groups. Then the mixture was filtered, washed with excess water, and finally dried at 50 °C under vacuum. The white solid obtained was denoted as HCMP-AO.

2.5. Uranium Adsorption. Aqueous solutions of uranium with different concentrations were obtained by diluting the saturated uranyl nitrate solution with deionized water. The pH value of uranium solution was adjusted with 0.1 mol/L HNO_3 or 0.1 mol/L NaOH. 10 mmol/L $NaClO_4$ was added to increase the ion strength. The concentrations of uranium solution were determined by a UV spectrophotometer, and the arsenazo III coloration method was employed in the test. Different concentrations of uranium solution at 1, 2, 4, and 5 ppm were prepared to determine the standard curve.

2.5.1. Influence of pH Value. The HCMP adsorbents were treated with a (3 wt %) KOH solution (100 mg of adsorbent per 100 mL of KOH solution) before adsorption experiments. To evaluate the influence of the pH value on the adsorption behavior, 4 mg of adsorbent and 20 mL of uranium solution (20 ppm) with a pH value varying from 2 to 7 were added into glass bottles followed by magnetic stirring at room temperature overnight. After separation of the adsorbents by using a syringe filter (0.45 μm membrane filter), the concentration of residual uranyl ions in the solution was measured by a UV spectrophotometer. The equilibrium adsorption capacity q_e (mg/g) was calculated by the following equation

$$q_e = \frac{(C_0 - C_e)V}{m} \tag{1}$$

where C_0 and C_e are the initial and equilibrium concentrations of uranyl ions, respectively, V is the volume of uranium solution, and m is the mass of adsorbent used in the test.

2.5.2. Uranium Sorption Kinetics. A uranium solution with a concentration of 20 ppm and pH of 6 was prepared by the method mentioned above. 4 mg of adsorbent and 200 mL of uranium solution were mixed in a glass bottle and stirred for 200 min at room temperature. At appropriate time intervals, 2.5 mL of mixture was taken and the adsorbents were separated. The uranium concentrations in the resulting solutions were analyzed by a UV spectrophotometer. The adsorption capacity q_t (mg/g) at different times were calculated by the following equation

$$q_t = \frac{(C_0 - C_t)V}{m} \tag{2}$$

where C_0 and C_t are the initial concentration and concentrations at t (min) of uranyl ions, respectively, V is the volume of uranium solution, and m is the mass of adsorbent used in the test.

2.5.3. Uranium Sorption Isotherm. To obtain the uranium sorption isotherm of HCMP-AO, 4 mg of HCMP-AO and 20 mL of uranium solution at different initial concentrations (10, 20, 50, 100, 160, and 200 ppm) were mixed in glass bottles and stirred at room temperature overnight. The initial and equilibrium concentrations of uranyl ions were measured by a UV spectrophotometer after separating the adsorbent by a syringe filter (0.45 μm membrane filter). The equilibrium adsorption capacity q_e (mg/g) at different concentrations were calculated by the following equation

$$q_e = \frac{(C_0 - C_e)V}{m} \tag{3}$$

where C_0 and C_e are the initial and equilibrium concentrations of uranyl ions, respectively, V is the volume of uranium solution, and m is the mass of adsorbent used in the test.

2.6. Density Functional Theory Calculation. The coordination mode and interaction energy between uranyl and the functional moiety were studied by density functional theory (DFT) using the Gaussian 09 code. The expanded boundless material limits the use of accurate quantum chemistry approaches. However, the bis-amidoxime functional moiety distributes separately on the expanded material, making it appropriate to model the interaction between the single bis-amidoxime moiety with uranyl, including the coordination mode, interaction energy, and the synergistic coordination effect. The structures of each possible coordination mode, the uranyl hydrated ion, and the representative bis-amidoxime ligand anion were optimized fully at the B3LYP level. The energy-consistent 5f-in-valence ECP60MWB and associated (14s13p10d8f6g)/[6s6p5d4f3g] valence basis set using a segmented contraction scheme were used for uranium. For all the ligand atoms, including C, N, O, and H, the 6-31G (d) basis set was used. For each optimized structure, analytical frequencies were calculated to ensure that the local minimum point on the potential energy surface was found. Solvent effects were taken into account implicitly with the SMD model.

2.7. Characterizations. Fourier transform infrared (FT-IR) spectra were recorded on a Bruker Vertex 70. Nitrogen sorption isotherms were measured at 77 K on a NOVA 3200e surface area and pore size analyzer. Before measurement, the samples were degassed in vacuum at 120 °C for 3 h. The Brunauer–Emmett–Teller (BET) method was utilized to calculate the specific surface areas. X-ray photoelectron spectroscopy (XPS) was performed by using a 250XI spectrometer with monochromatic X-ray source Al Kα excitation (1361 eV). Binding energy calibration was based on C 1s at 284.6 eV. Static water contact angles (CAs) were measured using the sessile drop method and image analysis of the drop file on a contact angle system (DSA30, Kruss GmbH). Scanning electron microscopy (SEM) images were collected using Hitachi SU 1510 and SU 4800 scanning electron microscopes. ^{13}C (125 MHz) cross-polarization magic-angle spinning (CP-MAS) was recorded on a Bruker Avance 500 spectrometer equipped with a magic-angle spin probe in a 4 mm (^{13}C) ZrO_2 rotor.

https://dx.doi.org/10.1021/acsami.9b20944
ACS Appl. Mater. Interfaces 2020, 12, 3688–3696

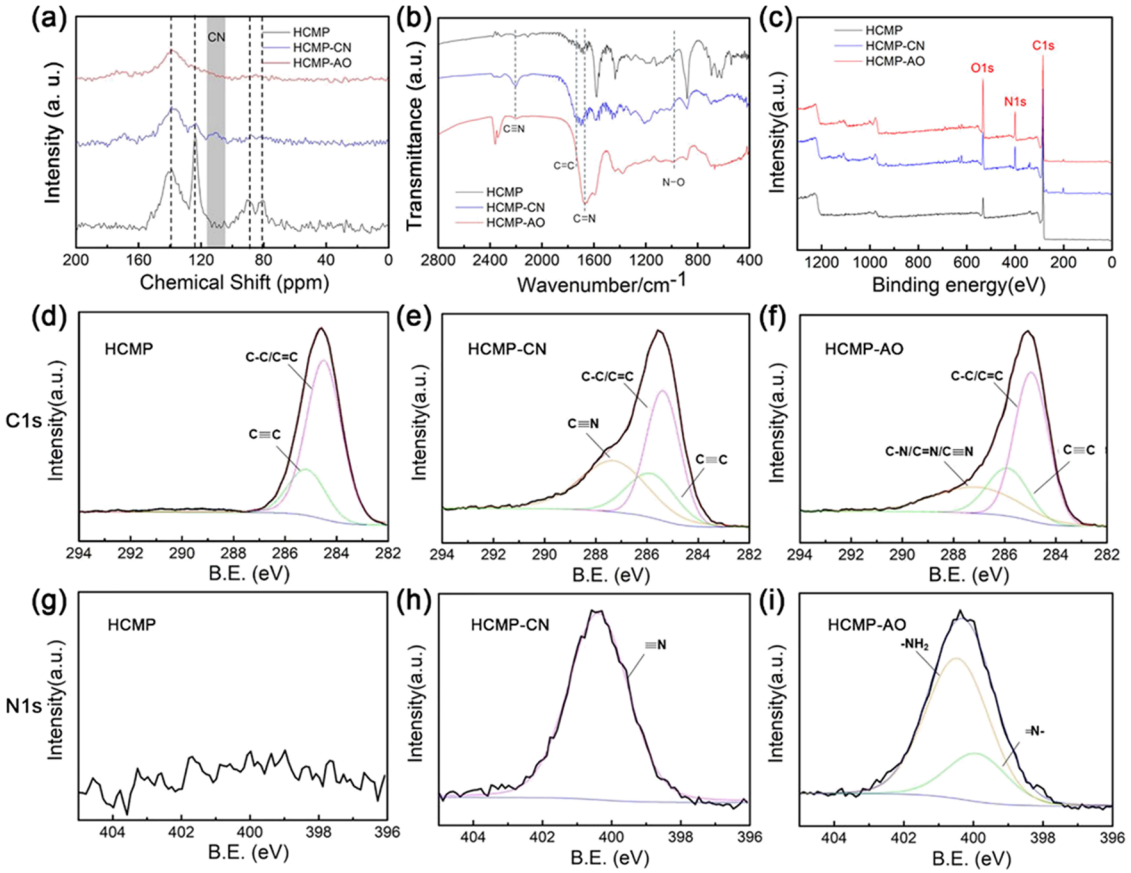

Figure 1. Solid-state ^{13}C NMR spectra (a), FT-IR spectra (b), full-scan XPS spectra (c), and high-resolution XPS spectra of C 1s (d–f) and N 1s (g–i) regions of the HCMPs.

3. RESULTS AND DISCUSSION

3.1. HCMP Synthesis and Characterizations. This work aims to develop an adaptable post-functionalization strategy by engineering the conjugated framework of CMPs to synthesize efficient adsorbents for uranium enrichment. Considering their large surface area and high structural regularity, HCMPs with well-defined 3D microporous networks were selected as a platform to accommodate functional moieties for the binding of uranyl ions. Scheme 1 shows the synthetic route of the HCMP adsorbents. Poly(phenylene butadiynylene) was synthesized via the Pd(II)/Cu(I)-catalyzed homocoupling polymerization of 1,3,5-triethynylbenzene.[32] The obtained HCMP consisted of 1,3,5-substituted benzene nodes connected by diyne struts. The abundant conjugated carbon–carbon triple bonds with approximately cylindrical π-electron delocalization along the rigid skeletons were then exploited to introduce cyano functionalities through an addition reaction with malononitrile. The intermediate, labeled as HCMP-CN, was finally subjected to hydroxylamine treatment in which the cyano groups were converted to bis-amidoxime uranophiles. The final product was named HCMP-AO.

Solid-state ^{13}C NMR spectroscopy was used to characterize the structure of the HCMPs (Figure 1a). The resonances at ~123 and ~140 ppm in the spectrum of intrinsic HCMP (black) were assigned to the C_{ar}–C and C_{ar}–H species. The peaks at ~ 89 and ~80 ppm correspond to the sp-hybridized $-C_{ar}-C\equiv C-$ and $-C\equiv C-C\equiv C-$ sites, respectively, the intensity of which evidently decreased after the addition reaction with malononitrile, accompanied by the appearance of a CN signal at ~112 ppm in the spectrum of HCMP-CN (blue). Then the CN signal disappeared in the spectrum of HCMP-AO (red) after the hydroxylamine treatment, suggesting the effective conversion of the CN groups to bis-amidoxime ligands. Supportive evidence was also provided by Fourier transform infrared (FT-IR) spectroscopy (Figure 1b). The stretching vibration signal of $-C\equiv C-$ at 2150 cm^{-1} decreased, and a strong band at 2300 cm^{-1} showed up in the spectrum of HCMP-CN, corresponding to the generation of CN groups in the intermediate. Meanwhile, signals of C=N (1666 cm^{-1}) and N–O (991 cm^{-1}) species were observed in the spectrum of HCMP-AO, indicating the transformation of the CN groups to amidoxime ligands.

X-ray photoelectron spectroscopy (XPS) was used to examine the surface chemistry of the HCMPs. According to the wide-scan spectra in Figure 1c, C 1s and O 1s signals were found for each sample. The N 1s signal was observed after the introduction of CN groups and their transformation to amidoxime ligands. The presence of O 1s signals in HCMP and HCMP-CN might be due to the adsorbed H_2O or CO_2 molecules on the surfaces of the homocoupling polymers. The signal of O 1s intensified in the spectrum of HCMP-AO after the cyano groups were converted to amidoxime groups. Table 1 summarizes the content of corresponding elements in the HCMPs based on XPS analysis.

High-resolution XPS spectra of C 1s and N 1s regions for the HCMPs are presented in Figure 1d–i. The C 1s regions can be divided into three kinds of species, namely, C–C/C=C (285.0 eV), C≡C (285.9 eV), and C–N/C=N/C≡N (287.1 eV), and the main species in HCMP are C–C/C=C and

https://dx.doi.org/10.1021/acsami.9b20944
ACS Appl. Mater. Interfaces 2020, 12, 3688–3696

Table 1. XPS Elemental Analysis and Nitrogen Adsorption−Desorption Measurements of HCMPs

sample	C (wt %)	N (wt %)	O (wt %)	U (wt %)	specific surface area (m^2/g)	pore volume (cm^3/g)
HCMP	89.2		10.8		1080	1.36
HCMP-CN	73.5	12.9	13.6		649	0.75
HCMP-AO	68.9	12.6	19.5		371	0.74
HCMP-AO (after adsorption)	47.3	5.6	22.0	25.1		

C≡C.[31] As cyano groups were introduced in the addition reaction, C≡N species were identified in the C 1s region of HCMP-CN. Table S1 gives the contents of the C−C/C=C, C≡C, and C≡N species. The peak profiles corresponding to the C 1s components basically remained constant during hydroxylamine treatment, with the dominant peaks attributed to C−N/C=N species. Accordingly, the N 1s regions can be divided into three kinds of species, namely, $-NH_2$ (400.5 eV), ≡N (400.4 eV), and =N− (399.9 eV).[51] In accordance with the analysis of C 1s regions, no N species is observed in HCMP and the peak at 400.4 eV corresponds to the cyano groups in HCMP-CN. Two component signals at 400.5 and 399.9 eV after hydroxylamine treatment are attributed to the $-NH_2$ and =N− species in amidoxime ligands.

The HCMPs were amorphous and showed no evidence of long-range order. The scanning electron microscope (SEM) images of these porous polymers showed relatively uniform solid sub-micron spheres (Figure 2a−c). Compared with the pristine HCMP, the introduction of cyano groups followed by their transformation to amidoxime moieties afforded smaller particles with rough surfaces. The surface wettability of these HCMPs was evaluated by performing the water contact angle measurement. Pristine HCMP exhibited nearly superhydrophobic surfaces with a CA of 147° (Figure 2d). The surface superhydrophobicity is attributed to the microporous structure and the hydrophobic polymer networks consisting of only aromatic rings and conjugated carbon−carbon triple bonds.[35] Post-functionalization of the HCMP significantly improved the surface hydrophilicity. Both HCMP-CN and HCMP-AO showed a CA less than 10° (Figure 2e,f). This would promote the dispersion of the HCMPs in aqueous solutions while benefiting their contact with the hydrophilic targets in the adsorption applications.

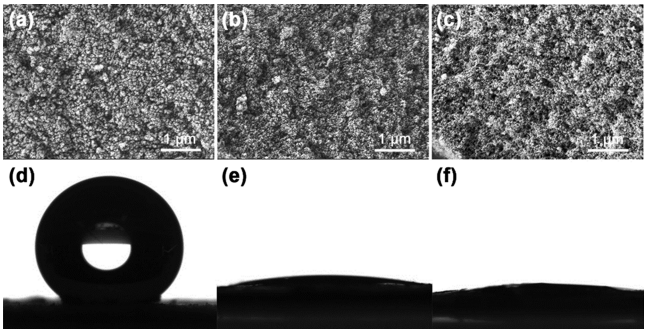

Figure 2. Morphologies of HCMP (a), HCMP-CN (b), and HCMP-AO (c) under SEM and the measurement of water contact angles for HCMP (d), HCMP-CN (e), and HCMP-AO (f).

Porosity of the HCMPs was investigated by nitrogen adsorption analysis. Figure 3a shows the nitrogen adsorption−desorption isotherms of HCMP, HCMP-CN, and HCMP-AO. Pronounced pore filling was observed at higher relative pressure with some significant hysteresis upon desorption, which was similar to previously reported CMPs.[32,34] With well-developed 3D microporous networks, the parent HCMP shows a high BET surface area of 1080 m^2/g. Subsequent skeleton engineering by addition reaction with malononitrile and hydroxylamine treatment resulted in a decrease in BET surface area and pore volume (Table 1). However, the final product HCMP-AO still possessed a high BET specific surface area of 371 m^2/g and pore volume of 0.74 cm^3/g. Thermogravimetric analysis (TGA) was used to study the thermostability of the HCMPs (Figure 3b). Due to the all-rigid conjugated framework nature, HCMP exhibited high thermal stability with T_{dec} > 300 °C. The functionalized counterparts after introducing the cyano groups and amidoxime ligands showed slight weight loss in the early stage in the TGA curves, which might be attributed to the removal of the adsorbed water on the samples.

3.2. Uranium Adsorption. The adsorption behavior of the HCMP adsorbents toward uranyl ions in aqueous solutions was investigated in a series of batch experiments. First, the effect of the pH value on the adsorption efficiency of the HCMPs was examined. The pH value basically influences the proton dissociation equilibrium of amidoxime ligands in solutions and their binding manner to uranyl ions. The optimal pH value for the highest adsorption capacity toward uranyl ions was determined to be 6 (Figure 4a), which agrees with a previous report.[10] Compared with the intrinsic HCMP and HCMP-CN, HCMP-AO exhibited much higher adsorption capacity, suggesting the effective binding ability of the bis-amidoxime ligands to uranyl ions.

The adsorption capacity variation of HCMP-AO upon contact with uranyl ions is shown in Figure 4b. A fast kinetics

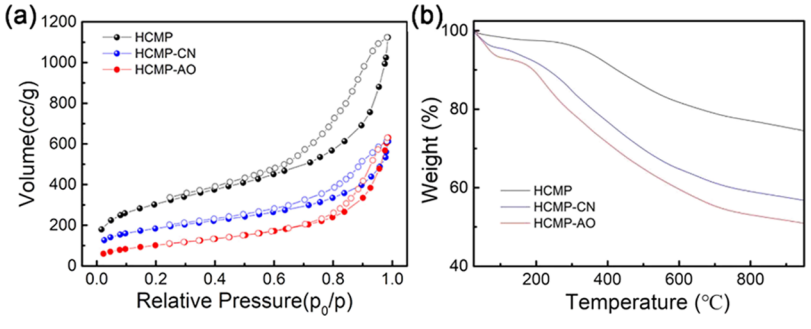

Figure 3. Nitrogen adsorption−desorption measurements (a) and TGA analysis (b) of HCMP, HCMP-CN, and HCMP-AO.

https://dx.doi.org/10.1021/acsami.9b20944
ACS Appl. Mater. Interfaces 2020, 12, 3688−3696

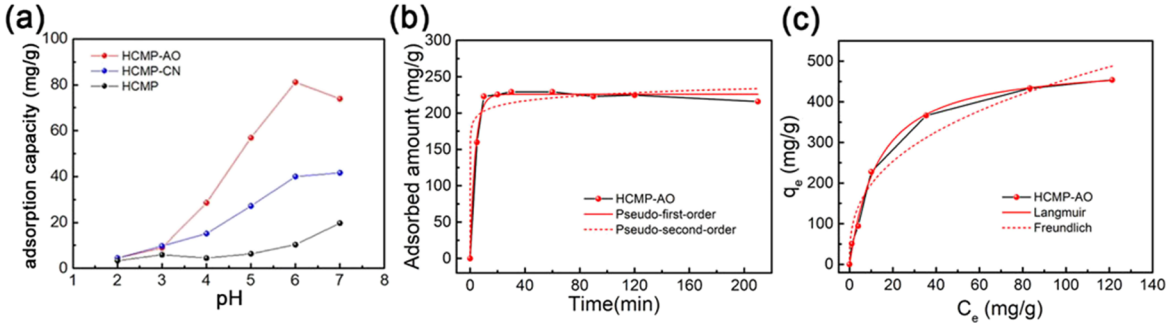

Figure 4. pH dependence of adsorption capacity of HCMP, HCMP-CN, and HCMP-AO in 20 ppm uranium solution for a contact time of 200 min (a), kinetic curve of uranium adsorption by HCMP-AO at pH = 6 (b), and influence of uranium concentration on the adsorption capacity of HCMP-AO (c).

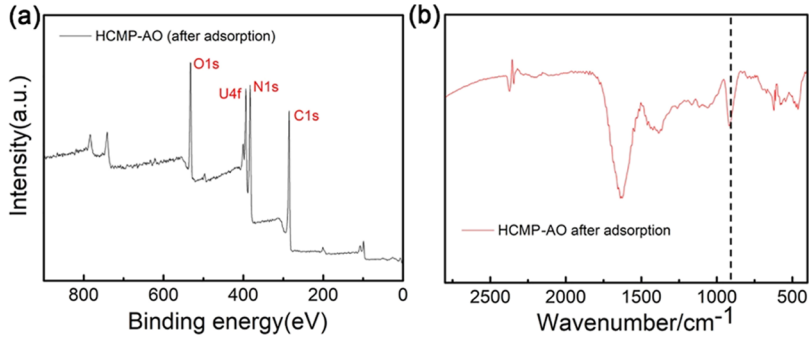

Figure 5. XPS spectra (a) and FT-IR spectra (b) of HCMP-AO after adsorption.

was observed with the adsorption equilibrium reaching within only 15 min. This should be attributed to the structural advantages of HCMPs with open and interconnected microporous networks, which benefited the diffusion of the uranyl ions and their contact with the amidoxime ligands. The adsorption capacity at equilibrium in 20 ppm uranium solution was about 230 mg/g. The adsorption procedure can be well fitted with the pseudo-first-order kinetic model with a calculated equilibrium capacity of 225.86 mg/g, as listed in Table S2. To assess the overall capacity, an adsorption isotherm (Figure 4c) was collected by equilibrating the HCMP-AO with a wide range of uranium concentrations from 10 to 200 ppm at a phase ratio of 0.2 mg/mL. A continuous increase of uranium adsorption with augmentation of the initial uranium concentrations was observed. The saturated adsorption capacity of HCMP-AO was about 450 mg/g, showing a superior performance to most of the traditional porous adsorbents. The Langmuir and Freundlich adsorption isotherm models were employed to fit the experimental data, and the calculated parameters are listed in Table S3. Apparently, the Langmuir model gives a better fitting result with a higher correlation coefficient R^2 of 0.995.

The structure of HCMP-AO after adsorption of uranyl ions was examined by XPS survey and FT-IR spectroscopy. The adsorbed uranyl ions were evidenced by the emergence of the U 4f signal in the wide-scan XPS spectrum of the recovered HCMP-AO from the uranium solutions, accompanied by the intensity increase of the O 1s signal (Figure 5a). Meanwhile, the characteristic peak at 912 cm^{-1} corresponding to uranyl ions was observed in the FT-IR spectrum (Figure 5b). These results proved the successful binding of uranium by HCMP-AO.

3.3. DFT Study on Coordination Mechanism. The underlying mechanism for the efficient binding of uranyl ions by the bis-amidoxime-functionalized HCMP is probed based on DFT calculation. First, electrostatic potential surfaces of the bis-amidoxime model molecule were obtained. Figure 6a shows

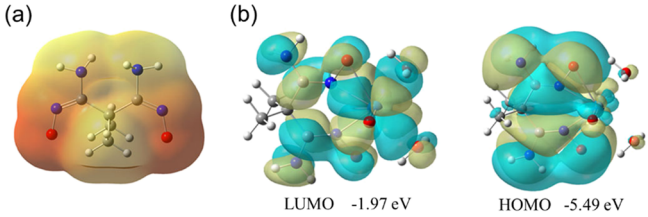

Figure 6. Calculated molecular electrostatic potential surfaces (a) and HOMO and LUMO diagrams for the uranyl/bis-amidoxime complex in synergistic coordination mode (b).

an evident negative charge distributed in the N−O regions, which is favored by uranyl ions to form complexation. The HOMO and LUMO diagrams revealed the interaction between the 5f orbital of U and 2p orbitals of N or O (Figure 6b). The 5f valence orbital of U overlaps with the 2p orbitals of the donor atoms, indicating evident covalency in the coordination bond of the uranyl/bis-amidoxime complex. This is in accordance with the previously observed strong complexation/adsorption ability of amidoxime ligands.

Basically, bis-amidoxime ligands can interact with uranyl ions in either synergistic coordination mode or individual coordination mode (Figure 7). The structures for uranyl/bis-amidoxime complexes taking synergistic coordination mode or individual coordination mode were optimized by DFT calculations, aiming to analyze the most energetically favored

https://dx.doi.org/10.1021/acsami.9b20944
ACS Appl. Mater. Interfaces 2020, 12, 3688−3696

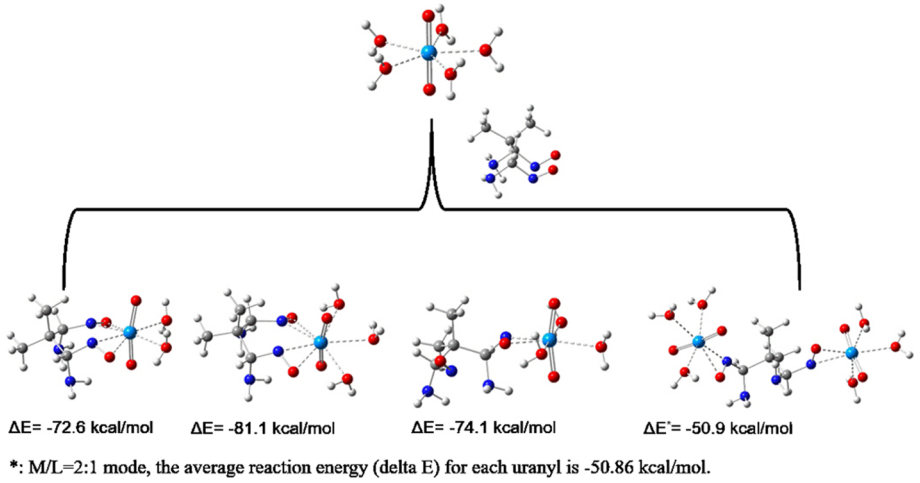

Figure 7. Reaction energies for different coordination modes based on DFT calculation.

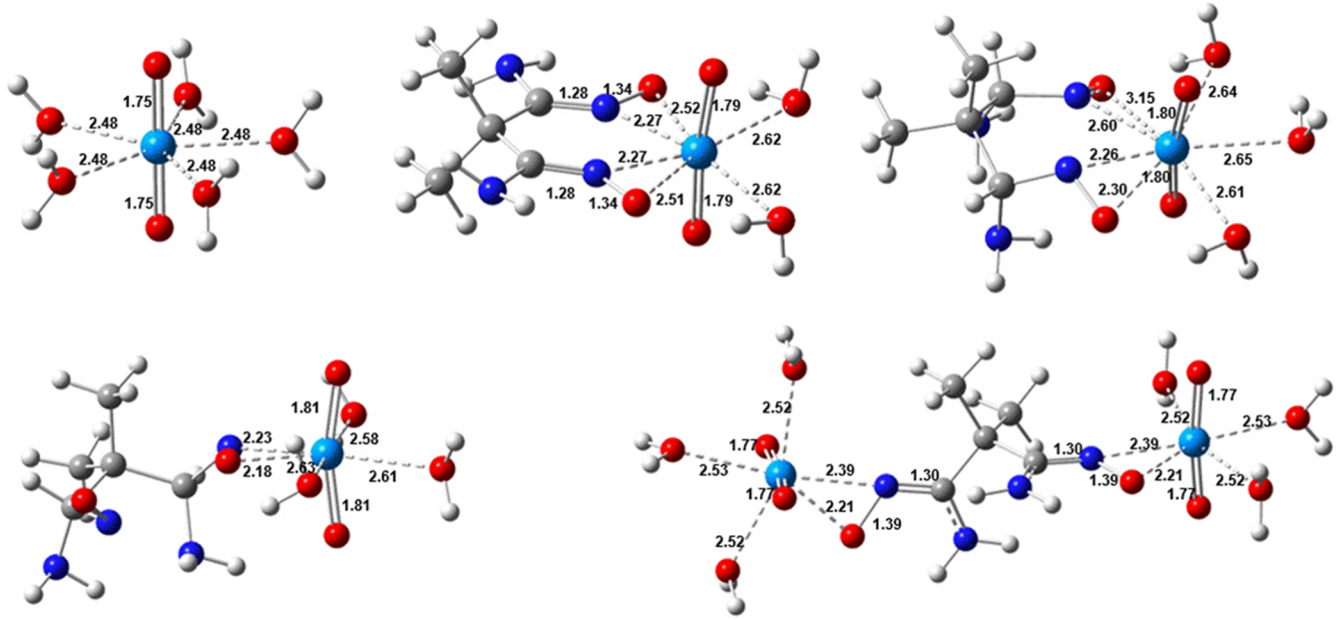

Figure 8. Optimized structures for uranyl/bis-amidoxime complexes taking different coordination modes.

coordination mode. As shown in Figure 8, the length of the axial U=O bond in the uranyl hydrated ion is about 1.75 Å while stretching to 1.77−1.78 Å in 2:1 (M/L) species and 1.80−1.81 Å in 1:1 species. The stretching in axial U=O bond length arises from the attack of bis-amidoxime in the equatorial plane, which weakens the axial U=O bond. This phenomenon further supports that bis-amidoxime has strong interaction with uranyl ions.

For the synergistic coordination mode, the reactions for bis-amidoxime replacing three or two water molecules are modeled. The reaction energies (ΔE) are −72.6 and −81.1 kcal/mol, respectively, indicating that bis-amidoxime ligands prefer to replace two water molecules of the uranyl hydrated ion. For individual coordination mode, the reaction energy is −74.1 kcal/mol when forming 1:1 species. It is also considered that the bis-amidoxime grasps uranyl on each, forming 2:1 (M/L) species. The reaction process is considered as $UO_2(H_2O)_5^{2+} + L^{2-} \rightarrow [UO_2(H_2O)_3LUO_2(H_2O)_3]^{2-} + 4H_2O$ (L = bis-amidoxime anion), where ΔE for the above reaction is −101.7 kcal/mol and the average reaction energy is only −50.9 kcal/mol for each uranyl. Thus, according to the DFT calculation, the bis-amidoxime ligands energetically favor to coordinate toward uranyl ions in a synergistic coordination manner. However, there is still the possibility that the uranyl/bis-amidoxime complexes take an individual coordination mode under the situation of high adsorption capacity.

4. CONCLUSIONS

In summary, we developed a new post-functionalization strategy for the synthesis of HCMP adsorbents for highly efficient uranium adsorption. HCMPs with well-developed microporous 3D networks were exploited as a reactive platform. Bis-amidoxime uranophiles were introduced through the engineering of their π-conjugated skeletons. The functionalized HCMP (HCMP-AO) preserved the open and interconnected microporous networks and high specific surface area (371 m^2/g). Due to the strong binding ability of the bis-amidoxime ligands, HCMP-AO exhibited high adsorption efficiency toward the uranyl ion in aqueous solutions with an optimal pH value of 6. The structural advantages of HCMP-

https://dx.doi.org/10.1021/acsami.9b20944
ACS Appl. Mater. Interfaces 2020, 12, 3688−3696

AO also guaranteed very fast adsorption kinetics within 15 min and high saturated capacity of about 450 mg/g. Moreover, the coordination mechanism between the bis-amidoxime ligands and uranyl ions was probed by DFT calculation, suggesting that a synergistic coordination might be the most energetically favored coordination mode of the uranyl/bis-amidoxime complexes. Overall, this study sheds light on the underlying principles attributed to the superior adsorption performance of HCMP adsorbents. Meanwhile, the synthetic strategy established here could be extended to task-specific design and synthesis of more functional HCMPs for broadened applications.

■ ASSOCIATED CONTENT

Supporting Information

The Supporting Information is available free of charge at https://pubs.acs.org/doi/10.1021/acsami.9b20944.

Contents of the C−C/C=C, C≡C, and C≡N species. Fitted kinetic and isotherm parameters of uranium adsorption by HCMP-AO. The coordinates of optimized structures of uranyl complexes by DFT methods (PDF)

■ AUTHOR INFORMATION

Corresponding Authors

Gang Ye − *Tsinghua University, Beijing, China;* orcid.org/0000-0002-7066-940X; Email: yegang@mail.tsinghua.edu.cn

Shengming Xu − *Tsinghua University, Beijing, China;* orcid.org/0000-0002-6765-9251; Email: smxu@tsinghua.edu.cn

Shengqian Ma − *University of South Florida, Tampa, Florida;* orcid.org/0000-0002-1897-7069; Email: sqma@usf.edu

Other Authors

Lei Zhang − *Tsinghua University, Beijing, China, and University of South Florida, Tampa, Florida*

Ning Pu − *Tsinghua University, Beijing, China*

Boxuan Yu − *Tsinghua University, Beijing, China*

Jing Chen − *Tsinghua University, Beijing, China*

Complete contact information is available at: https://pubs.acs.org/10.1021/acsami.9b20944

Notes

The authors declare no competing financial interest.

■ ACKNOWLEDGMENTS

The study was supported by the National Natural Science Foundation of China under Project 51673109, the Changjiang Scholars and Innovative Research Team in University (IRT13026), and the National Science Fund for Distinguished Young Scholars (51425403).

■ REFERENCES

(1) Abney, C. W.; Mayes, R. T.; Saito, T.; Dai, S. Materials for the Recovery of Uranium from Seawater. *Chem. Rev.* **2017**, *117*, 13935−14013.

(2) Lu, Y. Uranium extraction: Coordination chemistry in the ocean. *Nat. Chem.* **2014**, *6*, 175−177.

(3) Liu, C.; Hsu, P.-C.; Xie, J.; Zhao, J.; Wu, T.; Wang, H.; Liu, W.; Zhang, J.; Chu, S.; Cui, Y. A half-wave rectified alternating current electrochemical method for uranium extraction from seawater. *Nat. Energy* **2017**, *2*, 17007.

(4) Sun, Y.; Wu, Z.-Y.; Wang, X.; Ding, C.; Cheng, W.; Yu, S.-H.; Wang, X. Macroscopic and Microscopic Investigation of U(VI) and Eu(III) Adsorption on Carbonaceous Nanofibers. *Environ. Sci. Technol.* **2016**, *50*, 4459−4467.

(5) Parker, B. F.; Zhang, Z.; Rao, L.; Arnold, J. An overview and recent progress in the chemistry of uranium extraction from seawater. *Dalton Trans.* **2018**, *47*, 639−644.

(6) Wang, L.; Song, H.; Yuan, L.; Li, Z.; Zhang, Y.; Gibson, J. K.; Zheng, L.; Chai, Z.; Shi, W. Efficient U(VI) Reduction and Sequestration by Ti2CTx MXene. *Environ. Sci. Technol.* **2018**, *52*, 10748−10756.

(7) Li, Z.-J.; Huang, Z.-W.; Guo, W.-L.; Wang, L.; Zheng, L.-R.; Chai, Z.-F.; Shi, W.-Q. Enhanced Photocatalytic Removal of Uranium(VI) from Aqueous Solution by Magnetic TiO2/Fe3O4and Its Graphene CompositeEnhanced Photocatalytic Removal of Uranium(VI) from Aqueous Solution by Magnetic TiO2/Fe3O4 and Its Graphene Composite. *Environ. Sci. Technol.* **2017**, *51*, 5666−5674.

(8) Ivanov, A. S.; Parker, B. F.; Zhang, Z.; Aguila, B.; Sun, Q.; Ma, S.; Jansone-Popova, S.; Arnold, J.; Mayes, R. T.; Dai, S.; Bryantsev, V. S.; Rao, L.; Popovs, I. Siderophore-inspired chelator hijacks uranium from aqueous medium. *Nat. Commun.* **2019**, *10*, 819.

(9) Luo, W.; Xiao, G.; Tian, F.; Richardson, J. J.; Wang, Y.; Zhou, J.; Guo, J.; Liao, X.; Shi, B. Engineering robust metal-phenolic network membranes for uranium extraction from seawater. *Energy Environ. Sci.* **2019**, *12*, 607−614.

(10) Song, Y.; Ye, G.; Lu, Y.; Chen, J.; Wang, J.; Matyjaszewski, K. Surface-Initiated ARGET ATRP of Poly(Glycidyl Methacrylate) from Carbon Nanotubes via Bioinspired Catechol Chemistry for Efficient Adsorption of Uranium Ions. *ACS Macro Lett.* **2016**, *5*, 382−386.

(11) Wang, D.; Song, J.; Wen, J.; Yuan, Y.; Liu, Z.; Lin, S.; Wang, H.; Wang, H.; Zhao, S.; Zhao, X.; Fang, M.; Lei, M.; Li, B.; Wang, N.; Wang, X.; Wu, H. Significantly Enhanced Uranium Extraction from Seawater with Mass Produced Fully Amidoximated Nanofiber Adsorbent. *Adv. Energy Mater.* **2018**, *8*, 1802607.

(12) Yang, Y.; Wang, J.; Wu, F.; Ye, G.; Yi, R.; Lu, Y.; Chen, J. Surface-initiated SET-LRP mediated by mussel-inspired polydopamine chemistry for controlled building of novel core-shell magnetic nanoparticles for highly-efficient uranium enrichment. *Polym. Chem.* **2016**, *7*, 2427−2435.

(13) Yue, Y.; Mayes, R. T.; Kim, J.; Fulvio, P. F.; Sun, X. G.; Tsouris, C.; Chen, J.; Brown, S.; Dai, S. Seawater uranium sorbents: preparation from a mesoporous copolymer initiator by atom-transfer radical polymerization. *Angew. Chem., Int. Ed. Engl.* **2013**, *52*, 13458−13462.

(14) Zheng, T.; Yang, Z.; Gui, D.; Liu, Z.; Wang, X.; Dai, X.; Liu, S.; Zhang, L.; Gao, Y.; Chen, L.; Sheng, D.; Wang, Y.; Diwu, J.; Wang, J.; Zhou, R.; Chai, Z.; Albrecht-Schmitt, T. E.; Wang, S. Overcoming the crystallization and designability issues in the ultrastable zirconium phosphonate framework system. *Nat. Commun.* **2017**, *8*, 15369.

(15) Zhang, H.; Liu, W.; Li, A.; Zhang, D.; Li, X.; Zhai, F.; Chen, L.; Chen, L.; Wang, Y.; Wang, S. Three Mechanisms in One Material: Uranium Capture by a Polyoxometalate−Organic Framework through Combined Complexation, Chemical Reduction, and Photocatalytic Reduction. *Angew. Chem.* **2019**, *131*, 16256−16260.

(16) Wu, F.; Pu, N.; Ye, G.; Sun, T.; Wang, Z.; Song, Y.; Wang, W.; Huo, X.; Lu, Y.; Chen, J. Performance and Mechanism of Uranium Adsorption from Seawater to Poly(dopamine)-Inspired Sorbents. *Environ. Sci. Technol.* **2017**, *51*, 4606−4614.

(17) Mellah, A.; Chegrouche, S.; Barkat, M. The removal of uranium(VI) from aqueous solutions onto activated carbon: kinetic and thermodynamic investigations. *J. Colloid Interface Sci.* **2006**, *296*, 434−441.

(18) Chouyyok, W.; Pittman, J. W.; Warner, M. G.; Nell, K. M.; Clubb, D. C.; Gill, G. A.; Addleman, R. S. Surface functionalized nanostructured ceramic sorbents for the effective collection and

recovery of uranium from seawater. *Dalton Trans.* **2016**, *45*, 11312−11325.
(19) Carboni, M.; Abney, C. W.; Liu, S.; Lin, W. Highly porous and stable metal-organic frameworks for uranium extraction. *Chem. Sci.* **2013**, *4*, 2396−2402.
(20) Sun, Q.; Aguila, B.; Ma, S. Opportunities of Porous Organic Polymers for Radionuclide Sequestration. *Trends Chem.* **2019**, 292.
(21) Xu, H.; Gao, J.; Jiang, D. Stable, crystalline, porous, covalent organic frameworks as a platform for chiral organocatalysts. *Nat. Chem.* **2015**, *7*, 905−912.
(22) Lohse, M. S.; Bein, T. Covalent Organic Frameworks: Structures, Synthesis and Applications. *Adv. Funct. Mater.* **2018**, *28*, 1705553.
(23) Song, Y.; Sun, Q.; Aguila, B.; Ma, S. Opportunities of Covalent Organic Frameworks for Advanced Applications. *Adv. Sci.* **2019**, *6*, 1801410.
(24) Lu, Q.; Ma, Y.; Li, H.; Guan, X.; Yusran, Y.; Xue, M.; Fang, Q.; Yan, Y.; Qiu, S.; Valtchev, V. Postsynthetic Functionalization of Three-Dimensional Covalent Organic Frameworks for Selective Extraction of Lanthanide Ions. *Angew. Chem. Int. Ed. Engl.* **2018**, *57*, 6042−6048.
(25) McKeown, N. B.; Makhseed, S.; Budd, P. M. Phthalocyanine-based nanoporous network polymers. *Chem. Commun.* **2002**, 2780−2781.
(26) Xu, Y.; Jin, S.; Xu, H.; Nagai, A.; Jiang, D. Conjugated microporous polymers: design, synthesis and application. *Chem. Soc. Rev.* **2013**, *42*, 8012−8031.
(27) Li, M.; Ren, H.; Sun, F.; Tian, Y.; Zhu, Y.; Li, J.; Mu, X.; Xu, J.; Deng, F.; Zhu, G. Construction of Porous Aromatic Frameworks with Exceptional Porosity via Building Unit Engineering. *Adv. Mater.* **2018**, *30*, No. e1804169.
(28) Yuan, Y.; Zhu, G. Porous Aromatic Frameworks as a Platform for Multifunctional Applications. *ACS Cent. Sci.* **2019**, *5*, 409−418.
(29) McKeown, N. B.; Gahnem, B.; Msayib, K. J.; Budd, P. M.; Tattershall, C. E.; Mahmood, K.; Tan, S.; Book, D.; Langmi, H. W.; Walton, A. Towards polymer-based hydrogen storage materials: engineering ultramicroporous cavities within polymers of intrinsic microporosity. *Angew. Chem., Int. Ed. Engl.* **2006**, *45*, 1804−1807.
(30) Ben, T.; Pei, C.; Zhang, D.; Xu, J.; Deng, F.; Jing, X.; Qiu, S. Gas storage in porous aromatic frameworks (PAFs). *Energy Environ. Sci.* **2011**, *4*, 3991−3999.
(31) Han, S. S.; Furukawa, H.; Yaghi, O. M.; Goddard, W. A. Covalent Organic Frameworks as Exceptional Hydrogen Storage Materials. *J. Am. Chem. Soc.* **2008**, *130*, 11580−11581.
(32) Qian, H.-L.; Yang, C.-X.; Yan, X.-P. Bottom-up synthesis of chiral covalent organic frameworks and their bound capillaries for chiral separation. *Nat. Commun.* **2016**, *7*, 12104.
(33) Sun, Q.; Zhu, L.; Aguila, B.; Thallapally, P. K.; Xu, C.; Chen, J.; Wang, S.; Rogers, D.; Ma, S. Optimizing radionuclide sequestration in anion nanotraps with record pertechnetate sorption. *Nat. Commun.* **2019**, *10*, 1646.
(34) Sun, Q.; Tang, Y.; Aguila, B.; Wang, S.; Xiao, F. S.; Thallapally, P. K.; Al-Enizi, A. M.; Nafady, A.; Ma, S. Reaction Environment Modification in Covalent Organic Frameworks for Catalytic Performance Enhancement. *Angew. Chem., Int. Ed. Engl.* **2019**, *58*, 8670−8675.
(35) Li, X.; Wang, Z.; Sun, J.; Gao, J.; Zhao, Y.; Cheng, P.; Aguila, B.; Ma, S.; Chen, Y.; Zhang, Z. Squaramide-decorated covalent organic framework as a new platform for biomimetic hydrogen-bonding organocatalysis. *Chem. Commun.* **2019**, *55*, 5423−5426.
(36) Sun, Q.; Aguila, B.; Perman, J.; Ivanov, A. S.; Bryantsev, V. S.; Earl, L. D.; Abney, C. W.; Wojtas, L.; Ma, S. Bio-inspired nano-traps for uranium extraction from seawater and recovery from nuclear waste. *Nat. Commun* **2018**, *9*, 1644.
(37) Sun, Q.; Aguila, B.; Earl, L. D.; Abney, C. W.; Wojtas, L.; Thallapally, P. K.; Ma, S. Covalent Organic Frameworks as a Decorating Platform for Utilization and Affinity Enhancement of Chelating Sites for Radionuclide Sequestration. *Adv. Mater.* **2018**, *30*, 1705479.
(38) Li, B.; Sun, Q.; Zhang, Y.; Abney, C. W.; Aguila, B.; Lin, W.; Ma, S. Functionalized Porous Aromatic Framework for Efficient Uranium Adsorption from Aqueous Solutions. *ACS Appl. Mater. Interfaces* **2017**, *9*, 12511−12517.
(39) Aguila, B.; Sun, Q.; Cassady, H.; Abney, C. W.; Li, B.; Ma, S. Design Strategies to Enhance Amidoxime Chelators for Uranium Recovery. *ACS Appl. Mater. Interfaces* **2019**, *11*, 30919−30926.
(40) Jiang, J.-X.; Su, F.; Trewin, A.; Wood, C. D.; Campbell, N. L.; Niu, H.; Dickinson, C.; Ganin, A. Y.; Rosseinsky, M. J.; Khimyak, Y. Z.; Cooper, A. I. Conjugated microporous poly(aryleneethynylene) networks. *Angew. Chem. Int. Ed. Engl.* **2007**, *46*, 8574−8578.
(41) Cooper, A. I. Conjugated Microporous Polymers. *Adv. Mater.* **2009**, *21*, 1291−1295.
(42) Xu, M.; Han, X.; Wang, T.; Li, S.; Hua, D. Conjugated microporous polymers bearing phosphonate ligands as an efficient sorbent for potential uranium extraction from high- level liquid wastes. *J. Mater. Chem. A* **2018**, *6*, 13894−13900.
(43) Xu, M.; Wang, T.; Gao, P.; Zhao, L.; Zhou, L.; Hua, D. Highly fluorescent conjugated microporous polymers for concurrent adsorption and detection of uranium. *J. Mater. Chem. A* **2019**, *7*, 11214−11222.
(44) Jiang, J.-X.; Su, F.; Niu, H.; Wood, C. D.; Campbell, N. L.; Khimyak, Y. Z.; Cooper, A. I. Conjugated microporous poly(phenylene butadiynylene)s. *Chem. Commun.* **2008**, 486−488.
(45) Schmidt, J.; Werner, M.; Thomas, A. Conjugated Microporous Polymer Networks via Yamamoto Polymerization. *Macromolecules* **2009**, *42*, 4426−4429.
(46) Dawson, R.; Laybourn, A.; Clowes, R.; Khimyak, Y. Z.; Adams, D. J.; Cooper, A. I. Functionalized Conjugated Microporous Polymers. *Macromolecules* **2009**, *42*, 8809−8816.
(47) Kiskan, B.; Weber, J. Versatile Postmodification of Conjugated Microporous Polymers Using Thiol-yne Chemistry. *ACS Macro Lett.* **2011**, *1*, 37−40.
(48) Vukovic, S.; Hay, B. P. De novo structure-based design of bis-amidoxime uranophiles. *Inorg. Chem.* **2013**, *52*, 7805−7810.
(49) Piechowicz, M.; Abney, C. W.; Thacker, N. C.; Gilhula, J. C.; Wang, Y.; Veroneau, S. S.; Hu, A.; Lin, W. Successful Coupling of a Bis-Amidoxime Uranophile with a Hydrophilic Backbone for Selective Uranium Sequestration. *ACS Appl. Mater. Interfaces* **2017**, *9*, 27894−27904.
(50) Stemper, J.; Tuo, W.; Mazarío, E.; Helal, A. S.; Djurovic, A.; Lion, C.; Chahine, J.-M. E. H.; Maurel, F.; Hémadi, M.; Le Gall, T. Synthesis of bis(amidoxime)s and evaluation of their properties as uranyl-complexing agents. *Tetrahedron* **2018**, *74*, 2641−2649.
(51) Zeng, Z.; Wen, M.; Ye, G.; Huo, X.; Wu, F.; Wang, Z.; Yang, J.; Matyjaszewski, K.; Lu, Y.; Chen, J. Controlled Architecture of Hybrid Polymer Nanocapsules with Tunable Morphologies by Manipulating Surface-Initiated ARGET ATRP from Hydrothermally Modified Polydopamine. *Chem. Mater.* **2017**, *29*, 10212−10219.

https://dx.doi.org/10.1021/acsami.9b20944
ACS Appl. Mater. Interfaces 2020, 12, 3688−3696